Evaluating temporal consistency of long-term global NDVI datasets for trend analysis

Feng Tian [a,b,*], Rasmus Fensholt [a], Jan Verbesselt [c], Kenneth Grogan [a], Stephanie Horion [a], Yunjia Wang [b]

[a] Department of Geosciences and Natural Resource Management (IGN), University of Copenhagen, Øster Voldgade 10, Copenhagen K 1350, Denmark
[b] School of Environment Science and Spatial Informatics, China University of Mining and Technology, Daxue Road 1, Xuzhou 221116, China
[c] Laboratory of Geo-Information Science and Remote Sensing, Wageningen University, Droevendaalsesteeg 3, Wageningen 6708 PB, The Netherlands

ABSTRACT

As a way to understand vegetation changes, trend analysis on NDVI (normalized difference vegetation index) time series data have been widely performed at regional to global scales. However, most long-term NDVI datasets are based upon multiple sensor systems and unsuccessful corrections related to sensor shifts potentially introduce substantial uncertainties and artifacts in the analysis of trends. The temporal consistency of NDVI datasets should therefore be evaluated before performing trend analysis to obtain reliable results. In this study we analyze the temporal consistency of multi-sensor NDVI time series by analyzing the co-occurrence between breaks in the NDVI time series and sensor shifts from GIMMS3g (Global Inventory Modeling and Mapping Studies 3rd generation), VIP3 (Vegetation Index and Phenology version 3), LTDR4 (Long Term Data Record version 4) and SPOT-VGT (Système Pour l'Observation de la Terre VEGETATION). Single sensor time series from MODIS (MODerate Resolution Imaging Spectroradiometer) Terra and Aqua are used as reference datasets. The global land surface is divided into six regions according to the world humidity zones and averaged NDVI time series in each region are analyzed separately using a multiple structural change detection approach. We find that artifacts exist in the VIP3 and LTDR4 NDVI datasets with an abrupt shift detected in all humidity zones coinciding with the shift from NOAA-9 to NOAA-11 in 1988 and that orbital drift effects are evident in arid regions, potentially introducing uncertainties in NDVI trend analysis. Platform/sensor change from VGT-1 to VGT-2 is found to cause a significant positive break in the SPOT-VGT NDVI time series. Potential artifacts exist in humid, dry-subhumid, semi-arid and hyper-arid regions of GIMMS3g NDVI, whereas no signs of artifacts are found in the arid region. Although temporal consistency throughout all examined datasets increases after 2000 due to the usage of advanced platforms and sensors, variations in NDVI values from 2010 to 2011 still result in different trends at global and regional scales.

© 2015 Elsevier Inc. All rights reserved.

1. Introduction

Monitoring vegetation change over time at regional to global scales using Earth Observation data has greatly improved our understanding of the changing planet. Derived from red and near-infrared band reflectance, the normalized difference vegetation index (NDVI) (Tucker, 1979) is an efficient indicator for vegetation monitoring due to its simplicity and close relation to vegetation productivity (Prince, 1991; Tucker, Vanpraet, Sharman, & Van Ittersum, 1985). Thus, several datasets provide NDVI products at various spatial and temporal resolutions from a suite of sensor systems (Didan, 2010; Huete et al., 2002; Maisongrande, Duchemin, & Dedieu, 2004; Tucker et al., 2005). Through trend analysis of these NDVI time series, both gradual greening/browning vegetation changes related to land degradation and abrupt vegetation declines due to fires, insect outbreaks, etc. have been found

(Bai, Dent, Olsson, & Schaepman, 2008; Boschetti et al., 2013; Goetz, Fiske, & Bunn, 2006). However, existing long-term NDVI datasets that are based upon multiple sensor systems and artifacts in time series may be introduced from unsuccessful corrections related to sensor shifts between platforms/sensors (van Leeuwen, Orr, Marsh, & Herrmann, 2006) thereby introducing substantial uncertainties in trend analysis results. The lack of field observations with sufficient spatio-temporal coverage limits the evaluation and correction of such artifacts (Wessels, van den Bergh, & Scholes, 2012).

The longest continuous record of NDVI data comes from AVHRR (Advanced Very High Resolution Radiometer) sensors onboard NOAA (National Oceanic and Atmospheric Administration) satellite series, starting in July 1981, which forms the basis of generating long-term NDVI products (Brown, Pinzon, Didan, Morisette, & Tucker, 2006). However, this data suffers from several well-known problems, such as orbit drift of NOAA-7 through NOAA-14 (Pinzon, Brown, & Tucker, 2005), vicarious post-launch sensor calibration (Nagaraja Rao & Chen, 1995, 1996), and inconsistency between AVHRR/2 (1981–2000) and AVHRR/3 (2000–present) (Latifovic, Pouliot, &

* Corresponding author.
E-mail addresses: feng.tian@ign.ku.dk, ftian2012@gmail.com (F. Tian), rf@ign.ku.dk (R. Fensholt), wyj4139@163.com (Y. Wang).

Dillabaugh, 2012; Pinzon & Tucker, 2014). Based on AVHRR observations, several NDVI datasets were produced using different data processing methods to alleviate these problems; for example, the Pathfinder AVHRR Land (PAL) (James & Kalluri, 1994), the Fourier-Adjustment, Solar zenith angle corrected, Interpolated Reconstructed (FASIR) (Los et al., 2000), the Global Inventory Modeling and Mapping Studies (GIMMS) (Pinzon & Tucker, 2014; Tucker et al., 2005), and the Land Long Term Data Record (LTDR) (Pedelty et al., 2007). However, unsuccessfully corrected artifacts of PAL data in Central Asia and LTDR version 3 data in Libyan Desert were reported (Beck et al., 2011; de Beurs & Henebry, 2004). Discrepancies in the results of browning or greening trends amongst the AVHRR based NDVI datasets (Alcaraz-Segura, Chuvieco, Epstein, Kasischke, & Trishchenko, 2010; Alcaraz-Segura, Liras, Tabik, Paruelo, & Cabello, 2010) also indicate the importance of the preprocessing methods selected to overcome time series artifacts related to the use of multiple AVHRR instruments. Newer sensors like the Système Pour l'Observation de la Terre VEGETATION (SPOT-VGT) (1998–2014), Terra-MODIS (2000–present) and Aqua-MODIS (2002–present) are designed to have more stable orbits and improved spectral configurations for vegetation monitoring. NDVI time series from these datasets have been extensively included in vegetation analysis (Boschetti et al., 2013; Horion, Fensholt, Tagesson, & Ehammer, 2014; Ivits, Horion, Fensholt, & Cherlet, 2014; Rasmussen, Fensholt, Fog, Rasmussen, & Yanogo, 2014; Yin, Udelhoven, Fensholt, Pflugmacher, & Hostert, 2012), but their time span are shorter than AVHRR based datasets and are also not free of calibration related problems. SPOT-VGT was observed to suffer from data discontinuity in a desert transect between the VGT-1 and VGT-2 sensors (Fensholt, Rasmussen, Nielsen, & Mbow, 2009) and several bands of the Terra-MODIS sensor are reportedly influenced by degradation (Wang et al., 2012). Recent datasets take advantage of both the unique long time span of AVHRR sensors and the later and more advanced sensors to generate combined long-term NDVI datasets, such as the Vegetation Index and Phenology Laboratory (VIPLab) combining LTDR AVHRR (1981–1999) and MODIS (2000–2011) (Barreto-Munoz, 2013; Didan, 2010). Such long-term data may potentially also be influenced by sensor/data inconsistency related problems.

Vegetation trend analysis approaches have recently evolved from linear analysis, e.g. least squares regression, Theil–Sen and Mann–Kendall (de Beurs & Henebry, 2005; Fernandes & Leblanc, 2005) to also include analysis accounting for non-linearity, such as wavelet analysis (Martínez & Gilabert, 2009), polynomial model (Jamali, Seaquist, Eklundh, & Ardö, 2014), BFAST (Breaks For Additive Seasonal and Trend) analysis (Verbesselt, Hyndman, Newnham, & Culvenor, 2010; Verbesselt, Hyndman, Zeileis, & Culvenor, 2010), and DBEST (Detecting Breakpoints and Estimating Segments in Trend) analysis (Jamali, Jönsson, Eklundh, Ardö, & Seaquist, 2015). These newly developed analyses are able to capture rapid and reversing vegetation changes in long term time series that risk to be balanced out in linear analyses (de Jong, Verbesselt, Schaepman, & de Bruin, 2012), thus enabling improved insights into vegetation responses to short term climatic changes and human activities. At the same time, however, the methods accounting for non-linear changes are more sensitive to abrupt changes or short period of trends, thus potentially confusing actual vegetation changes by unsuccessfully corrected sensor artifacts. Therefore, in order to obtain reliable results of vegetation changes, trend analysis should not be performed with temporally inconsistent NDVI datasets characterized by significant abrupt changes or short period of trends caused by incomplete sensor cross-calibration or inadequate correction of known issues, such as orbital drift and sensor degradation.

The aim of this study is to identify potential sensor related artifacts in GIMMS3g, VIP version 3 (VIP3), LTDR version 4 (LTDR4) and SPOT-VGT NDVI datasets. The global NDVI datasets from MOD13C2, MYD13C2, LTDR-Terra and LTDR-Aqua are also included as references in the study as they do not include platform/sensor shifts. Analyses of individual dataset are performed using a multiple structural change detection algorithm under the assumptions that 1) the influence of artifacts in NDVI time series are most easily detectable through averaging on a regional to global scale and 2) the severity of artifacts, as well as the corresponding corrections applied, vary for different vegetation densities.

2. Data

2.1. NDVI datasets

The AVHRR sensor based long-term NDVI datasets evaluated in this study are GIMMS3g, VIP3 and LTDR4. Table 1 provides detailed information on the processing details of each of the datasets. The time span covers from 1982 to 2011. The 15-day GIMMS3g data and daily LTDR4 data were aggregated to a monthly temporal resolution using maximum value compositing (MVC) method (Holben, 1986).

The SPOT-VGT S10 product provides 10-day MVC NDVI data from April 1998 to May 2014, covering from north 75° to south 56° at 1 km spatial resolution. This dataset is produced using observations from VGT-1 onboard SPOT-4 (April 1998–January 2003) and VGT-2 onboard SPOT-5 (February 2003–May 2014). SPOT-VGT S10 products have been corrected for atmospheric effects based on the SMAC (Simplified Model for Atmospheric Correction) algorithm (Maisongrande et al., 2004; Rahman & Dedieu, 1994). Differences in the spectral response function between VGT-1 and VGT-2 sensors can introduce between-sensor reflectance variations (VITO, 2014). We restricted the time span from 1999 to 2011 in this study. The data can be downloaded from http://www.vgt.vito.be/.

The MODIS sensor onboard the Terra platform (Terra-MODIS) has acquired data since February 2000 crossing the dayside equator at 10:30 am local time. The identical MODIS sensor onboard the Aqua platform (Aqua-MODIS) began operation two years later than Terra-MODIS and was put in an orbit with equator crossing time at 13:30 pm local time. Both MODIS time series are based on single sensors and are therefore not influenced by sensor shifts. The reference MODIS NDVI data includes the MOD13C2 (Collection 5), MYD13C2 (Collection 5), LTDR-Terra and LTDR-Aqua NDVI products. All selected data are processed as CMG's (Climate Modeling Grid) at a spatial resolution of 0.05° generated from MODIS land surface reflectance data being thoroughly corrected for atmospheric effects (Vermote, El Saleous, & Justice, 2002). BRDF (bidirectional reflectance distribution function) effects have been corrected for in the LTDR-Terra and LTDR-Aqua data, but not in the MOD13C2 and MYD13C2 data. However, as the orbits of both the Terra and Aqua platforms have been stable throughout the operating period, the BRDF effect should not make a difference for the MODIS data based inter-annual trend analysis as also shown by Guay et al. (2014). The MOD13C2 and MYD13C2 are monthly data temporally aggregated from the 16-day maximum composites using a weighted average (Solano, Didan, Jacobson, & Huete, 2010) and the period of use is restricted to 2001–2011 and 2003–2011, respectively, in this study. The LTDR-Terra and LTDR-Aqua data are daily observations and we aggregated these into monthly maximum values and used data during the periods of 2001–2011 and 2003–2011, respectively. The MOD13C2 and MYD13C2 can be obtained from http://reverb.echo.nasa.gov/, and the LTDR data are available from ftp://ltdr.nascom.nasa.gov/allData/MODIS2LTDR/.

2.2. World humidity zones

Systematic errors (e.g. orbital drift effects) in AVHRR data vary as a function of vegetation properties and location (Pinzon et al., 2005). Additionally, the quality of GIMMS NDVI data was reported to vary amongst different land cover classes when compared to MODIS NDVI data (Fensholt & Proud, 2012). Therefore, we evaluate the NDVI datasets in separate regions defined by the world humidity zones used as a proxy

Table 1
Processing details for the AVHRR based NDVI products evaluated in this study.

|	GIMMS3g	VIP3	LTDR4
Data input	AVHRR GAC level-1b data	LTDR3 AVHR09C1 and MOD09CMG data	AVHRR GAC level-1b data
Platform/sensor lineage	AVHRR-2: 01/1982–02/1985 NOAA-7 03/1985–10/1988 NOAA-9 11/1988–08/1994 NOAA-11 09/1994–12/1994 NOAA-9 01/1995–10/2000 NOAA-14 AVHRR-3: 11/2000–12/2003 NOAA-16 01/2004–12/2008 NOAA-17 01/2009–12/2011 NOAA-18	AVHRR-2 (LTDR3 AVHR09C1): 01/1982–12/1984 NOAA-7 01/1985–10/1988 NOAA-9 11/1988–09/1994 NOAA-11 01/1995–12/1999 NOAA-14 MOD09CMG: 02/2000–12/2011 Terra	AVHRR-2: 01/1982–12/1984 NOAA-7 01/1985–10/1988 NOAA-9 11/1988–09/1994 NOAA-11 01/1995–12/1999 NOAA-14 AVHRR-3: 01/2001–12/2006 NOAA-16 01/2007–12/2011 NOAA-18
Radiometric calibration	AVHRR-2: Ocean and clouds vicarious calibration (Vermote & Kaufman, 1995), followed by desert calibration for NDVI itself (Los, 1998) AVHRR-3: Operational NOAA–NESDIS (desert) vicarious calibration coefficients	LTDR3 AVHR09C1: Ocean and clouds vicarious calibration (Vermote & Kaufman, 1995) MOD09CMG: Onboard calibration (Xiong & Barnes, 2006)	Ocean and clouds vicarious calibration (Vermote & Kaufman, 1995)
Atmospheric correction	None, but extra aerosol correction was applied during El Chichon (04/1982–12/1984) and Mt Pinatubo (06/1991–12/1993) volcanic stratospheric aerosol periods (Vermote, Saleous, Kaufman, & Dutton, 1997)	Rayleigh scattering, ozone, water vapor, aerosol corrections	Rayleigh scattering, ozone, water vapor, aerosol corrections
BRDF correction	AVHRR-2: Adaptive empirical mode decomposition/reconstruction (Pinzon et al., 2005) AVHRR-3: none	LTDR3 AVHR09C1: The same method with MODIS BRDF correction (Schaaf et al., 2002) MOD09CMG: none	The same method with MODIS BRDF correction (Schaaf et al., 2002)
Temporal composting	15-day maximum	Daily, 7-day, 15-day, monthly maximum	Daily
Spatial resolution	1/12°.	0.05°	0.05°
Cloud screening	Channel 5 thermal mask of 0 °C (10 °C for Africa)	LTDR3 AVHR09C1: Channel 5 thermal mask of 0 °C MOD09CMG: Generated from combined MODIS bands information and ancillary data	Channel 5 thermal mask of 0 °C
Noise removal	Kriging interpolation	Larger than 1.5 standard deviations of long term averages	Fourier adjustment
Gap filling	Kriging interpolation	Inverse distance weighting interpolation (if failed using the long term average instead)	None
Sensor inter-calibration	Bayesian analysis using SeaWiFS NDVI as evidence information (Pinzon & Tucker, 2014)	Land cover based empirical equations	None
Main references	Pinzon & Tucker, 2014; Tucker et al., 2005	Barreto-Munoz, 2013; Didan, 2010; Pedelty et al., 2007	Pedelty et al., 2007
Data source	https://nex.nasa.gov/nex/projects/1314	http://measures.arizona.edu/vip_workshop_docs.php	http://ltdr.nascom.nasa.gov/cgi-bin/ltdr/ltdrPage.cgi
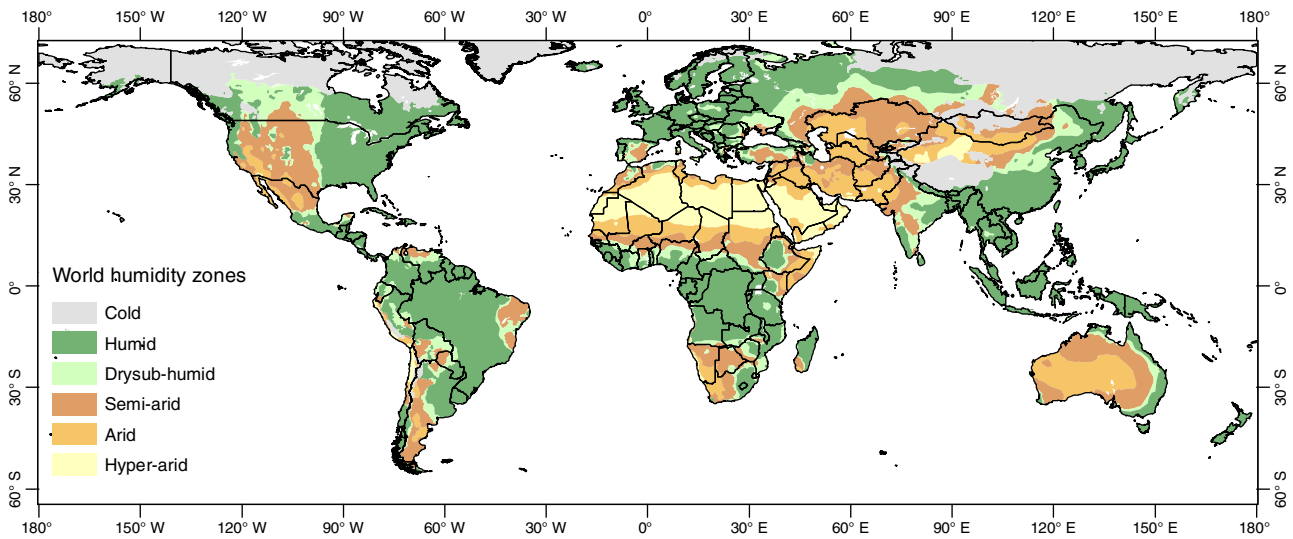
Fig. 1. World humidity zones defined by the United Nations Environment Program (UNEP).

for separating between different vegetation densities. The world humidity zones are defined by the United Nations Environment Program (UNEP) based on a global humidity index, as the ratio of annual precipitation and potential evapotranspiration (P/PET) (UNEP et al., 1997).

According to the mean annual potential moisture availability for the period 1951–1980, global land surface is classified into a humid zone (P/PET $\geq$ 0.65), dry-subhumid zone (0.65 > P/PET $\geq$ 0.50), semi-arid zone (0.50 > P/PET $\geq$ 0.20), arid zone (0.20 > P/PET $\geq$ 0.05) and a
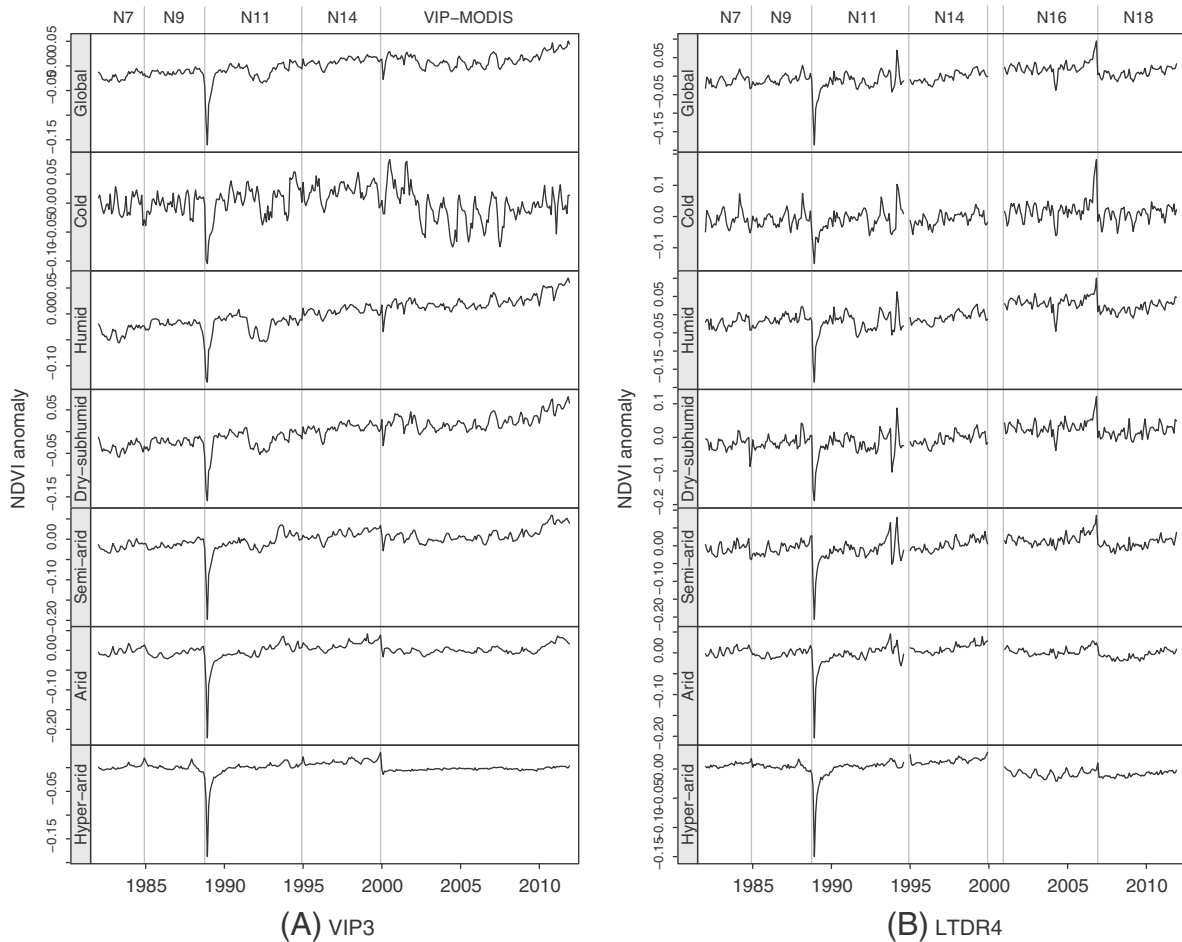

Fig. 2. NDVI anomalies of global and humidity zone averaged NDVI time series derived from (A) VIP3 and (B) LTDR4 datasets. The gray vertical lines denote satellite changing time (N means NOAA).

hyper-arid zone (P/PET < 0.05) (Fig. 1). The cold zone is defined as areas that have more than six months average temperature below 0 °C and not more than three months above 6 °C. All of the NDVI datasets are subset to the spatial extent shown in Fig. 1. The humidity zones map can be obtained from http://geonetwork. grid.unep.ch/.

3. Methods

3.1. Averaging NDVI data on global and regional scales

Detecting sensor related artifacts at the per-pixel level can be challenging because the magnitudes of NDVI changes caused by cloud contamination and actual land surface disturbance, i.e. fires, floods etc. can be much larger than those caused by unsuccessfully corrected artifacts, thus concealing the later. However, when averaging the NDVI values on a global or regional scale, cloud contamination and small scale actual changes are expected to be balanced out, making the detection of systematic bias/errors caused by cross sensor differences more easily detectable. Therefore, the evaluations were performed on both global and regional averaged NDVI time series for each of the humidity zones. Detected breaks were considered potential artifacts if they coincided with the satellite sensor changes. Consequently, the corresponding NDVI time series were deemed to be temporally inconsistent and should be used with caution for trend analysis. However, large scale events like El Niño/La Niña and the Mt Pinatubo volcanic eruption may also cause vegetation changes on global or regional scales (Anyamba & Eastman, 1996; Li & Kafatos, 2000; Lucht et al., 2002) and introduce breaks in the averaged NDVI time series. If a break was detected close to the dates of these natural events and the dates of sensor changes, it would be difficult to know which one was causing the break. In this case, those datasets being free or partly free from sensor shift (i.e. MODIS data and SPOT-VGT2) can provide references for discriminating between these two types of changes during the overlap periods. CO_2 fertilization impacts on global vegetation is not expected to introduce abrupt shifts in time series (Los, 2013; Mao et al., 2013) and is therefore not likely to be confused by time series breaks caused by satellite sensor shifts.

3.2. De-seasonalizing NDVI time series

Compared to the NDVI seasonal variations, even in arid regions, the magnitude of abrupt changes related to sensors are usually small. Therefore, the temporal consistency evaluation was performed on NDVI anomalies (the NDVI time series was de-seasonalized by subtracting the long-term average seasonal effects from the monthly values). It is clear from Fig. 2 that at the beginning of the NOAA-11 operating period, the NDVI anomalies are significantly below the normal level in all VIP3 and LTDR4 averaged series, indicating that NDVI data during this period is of sub-optimal quality in these datasets. Therefore, we excluded one year data from November 1988 to October 1989 in the analysis of VIP3 and LTDR4 (assuming the obvious bad quality data during this period) to better assess the quality of the remaining part of NOAA-11 time series. The years of 1994 and 2000 are also excluded from the analysis of LTDR4 data because of existing data gaps.

3.3. Detecting breaks in NDVI anomaly series

We employed the multiple structural change detection approach (Bai, 1997; Bai & Perron, 2003) for detecting breaks in the NDVI anomaly series. This method was firstly developed for characterizing long-term shift in economic time series data. Verbesselt, Hyndman, Newnham, et al. (2010) incorporated this approach into the BFAST tool for NDVI seasonal and trend change detection which has been applied in several studies (Forkel et al., 2013; Lambert, Drenou, Denux, Balent, & Cheret, 2013; Schucknecht, Erasmi, Niemeyer, &

Matschullat, 2013; Watts & Laffan, 2014). The NDVI anomaly series was modeled by the linear structural change model with m breaks ($m + 1$ segments)

$$y_i = a_j x_i + b_j + \varepsilon_i \quad \left(i = i_{j-1} + 1, ..., i_j; \; j = 1, ..., m+1\right) \qquad (1)$$

where j is the index of the segment, $(i_1, ..., i_m)$ represents the set of the break positions and by convention $i_0 = 0$, $i_{m+1} = n$ (n is the size of the time series), a and b are the regression coefficients that can be estimated by the ordinary least square method, and ε is the residual. For vegetation trend analysis, both the number and positions of breaks in a NDVI time series are unknown and have to be estimated from the data. Given a minimal number of observations in one segment (h), the maximum number of breaks allowed is no more than the ratio between h and the total number of observations in the time series (n). Each possible number of breaks represents one model to fit the NDVI anomaly data. For each specific number of breaks, all the possible sets of the break positions can be obtained through a standard grid search procedure. The optimal set of break positions is determined by minimizing the sum of squared residuals.

$$\left(\hat{i}_1, ..., \hat{i}_m\right) = arg \; \min_{(i_1, ..., i_m)} \sum_{i=1}^{n} \varepsilon_i. \qquad (2)$$

Bai (1997) constructed the distribution function for the break positions under an asymptotic framework where the magnitudes of the shifts between segments converge to zero as the size of the time series increases. For a given significance level, the confidence interval of each break was constructed based on the distribution function and the data of the two segments at both sides of the break. Once all the possible models have been set up, the optimal one was determined using the Bayesian Information Criterion (BIC) (Gideon, 1978). BIC was designed for model selection based on the information theory, calculated by

$$BIC = -2ln(L) + K \; log(n) \qquad (3)$$

where L is the maximum likelihood for the model and K is the number of parameters. The selected model is the one with the minimum BIC value.

When determining the optimal set of break positions, the extensive grid search for the global minimizers would be of order $O(n^m)$. To speed up the computation, Bai and Perron (2003) presented a dynamic programming algorithm using a recursive procedure that performs least square operations of order $O(n^2)$. This algorithm generates a triangular matrix of sums of squared residuals that contains all the possible segments (at most $n(n+1)/2$). Based on this triangular matrix, the global minimizers (the optimal set of break positions) for any number of breaks can be obtained, as well as the corresponding BIC values, regression coefficients and confidence intervals. The procedures described above were implemented with the function 'breakpoints' in the R package 'strucchange' (Zeileis & Kleiber, 2005; Zeileis, Kleiber, Krämer, & Hornik, 2003; Zeileis, Leisch, Hornik, & Kleiber, 2002).

The h parameter must be assigned prior to the breakpoints analysis. The results can potentially vary by setting different h parameters because it determines the minimal length of a segment (Zeileis & Kleiber, 2005). Using a low h value will produce more breaks in the time series as compared to a higher h value. When setting a h value larger than n/2, the analysis will give no breaks and become a simple linear trend analysis. Therefore, the h parameter should be selected according to the length of the time period between successive structural changes. In addition, a uniform h parameter should be used to ensure that all the statistical analyses are performed at the same significance level. In this study, we set the h to 24 (2 years) to allow the evaluation of temporal consistency for the shortest period covered by a single sensor. The confidence intervals of the detected breaks were calculated at a significance level of 0.05.
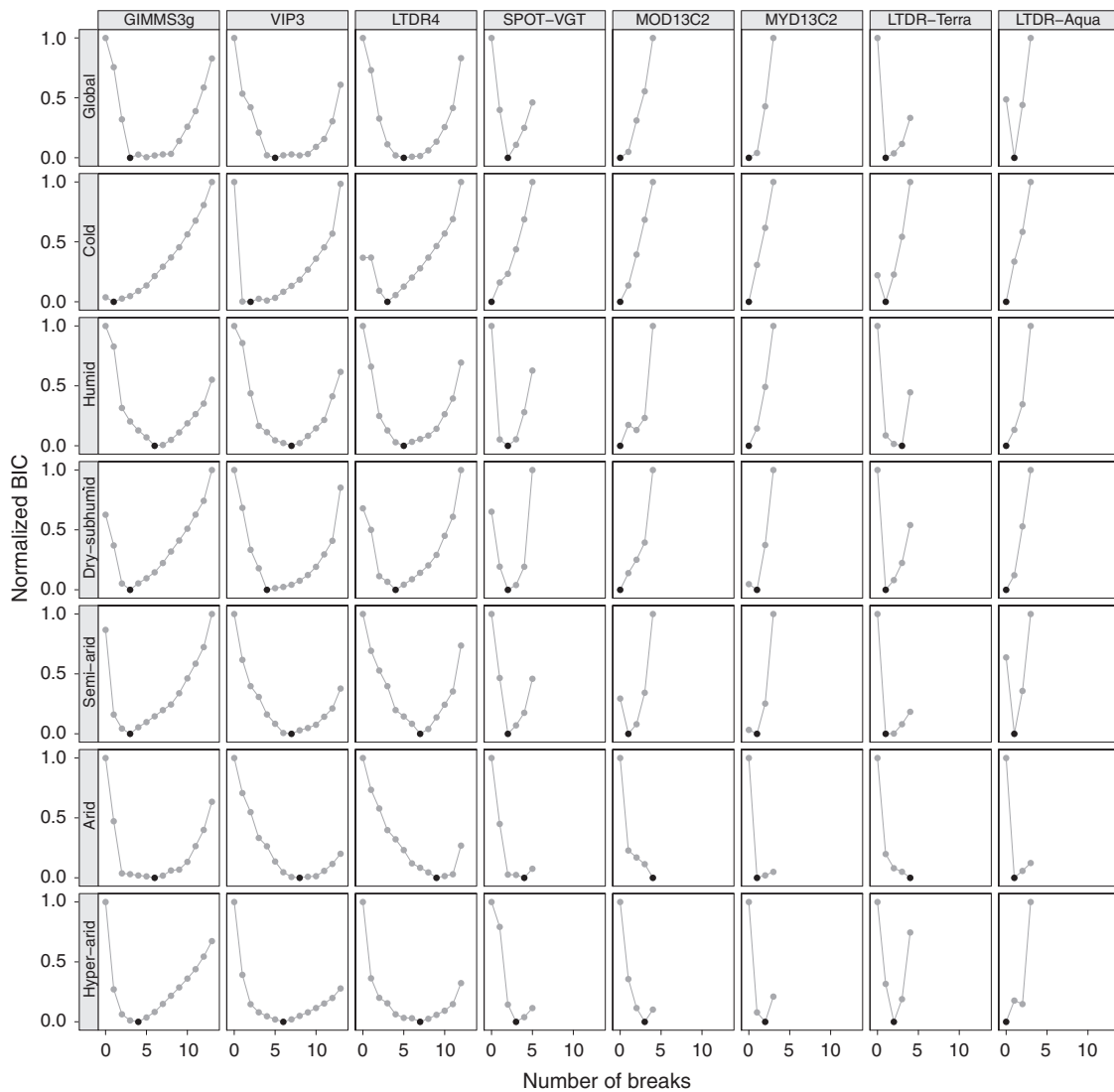
Fig. 3. Normalized BIC values for all possible number of breaks (model) in each NDVI anomaly series. The models with minimal values (black dots) are selected as being the optimal.

4. Results

For each NDVI anomaly series, all the possible fitted models (number of breaks) were calculated and Fig. 3 shows the associated BIC values for each model (normalized to 0–1 for improved visualization). There are fewer models calculated for SPOT-VGT, Terra, Aqua, LTDR-Terra and LTDR-Aqua time series than GIMMS3g, VIP3 and LTDR4 because their total number of observations are different. BIC shows clear differences between different models; the models with the minimal BIC values were selected and shown in Fig. 4. The magnitudes and dates of detected breaks and the corresponding confidence intervals are listed in Table 2.

Fig. 4A shows the results of the GIMMS3g averaged NDVI anomaly series data. The NOAA-7 to NOAA-9 sensor shift date is located in the narrow confidence interval of the first detected break in April 1985 (magnitude = 0.023) in the humid region and the NOAA-9 to NOAA-11 sensor shift date is close to the second detected break, however not coinciding with the break confidence interval. A break is detected during the NOAA-9 period in the arid zone but not close to either of these two sensor shifts. No breaks are detected around these two sensor shifts dates in the other humidity zones of the GIMMS3g data. Negative breaks are detected in averaged NDVI anomaly series of global, humid, dry-subhumid and semi-arid regions in June/July 1991 (with magnitudes

of −0.015, −0.025, −0.02 and −0.009, respectively) when GIMMS3g data starts including the correction of Mt Pinatubo volcano eruption effects. Positive breaks are detected in global, humid, dry-subhumid and arid regions around September 1994 (magnitudes of 0.015, 0.041, 0.018 and 0.009), coinciding with the sensor shift from NOAA-11 to NOAA-9 (descending). It should be noticed that another sensor shift from NOAA-9 (descending) to NOAA-14 is following shortly after in January 1995. Two breaks are detected in the middle of 1997 in humid and arid regions. The humid, semi-arid and hyper-arid regions show breaks coinciding with the NOAA-14 to NOAA-16 sensor shift in November 2000 (magnitudes of 0.017, −0.011 and 0.006). This sensor shift date is also located within the confidence interval of the detected break in March 2002 (magnitude = −0.012) in the dry-subhumid region. The NOAA-17 to NOAA-18 sensor shift date coincides with the detected break for the hyper-arid region in the end of 2008 (magnitude = 0.007) and aligns with the confidence interval of the detected break in June 2009 (magnitude = 0.008) for the global averaged series. Several breaks are detected during the NOAA-17 period, i.e. in April 2008 (magnitude = −0.002) for the semi-arid region, March 2005 (magnitude = 0.005) and December 2007 (magnitude = −0.012) for the arid region, and August 2004 (magnitude = 0.002) for the hyper-arid region, but no sensor shifts are overlapping break confidence intervals. All the series except for

the hyper-arid region show increasing trends after the last break detected.

Fig. 4B shows the results of the VIP3 data series excluding data from November 1988 to October 1989. The NOAA-7 to NOAA-9 sensor shift date coincides with the first detected break in 1985 for the humid, semi-arid, arid and hyper-arid regions (magnitudes of 0.013, −0.013, −0.028 and −0.009). Although we excluded the beginning of the NOAA-11 data, an overlap between detected breaks and the NOAA-9 to NOAA-11 sensor shift are still found in humid and arid regions (magnitudes of 0.023 and −0.016). Breaks coinciding with this sensor shift are also detected in global, dry-subhumid and hyper-arid regions (magnitudes of 0.015, 0.023 and −0.013). A notable drop of NDVI anomaly values at this sensor shift date is found in semi-arid region, but not detected as a break. During the period of NOAA-11, NDVI anomaly variation patterns are similar in global, humid and dry-subhumid regions, with detected abrupt changes in November 1992, five months after the Mt Pinatubo volcano eruption (magnitudes of 0.032, 0.039 and 0.038). In the semi-arid region, an abrupt decrease is detected in May 1991 (magnitude = −0.023), coinciding with the Mt Pinatubo volcano eruption, followed by an abrupt increase in May 1993 (magnitude = 0.033). Two breaks in 1991 and 1993 are detected in the arid regions (magnitudes of −0.005 and −0.015) that are less sharp as compared to the semi-arid region. The Hyper-arid region shows similar change patterns to the arid region. No breaks are detected around the NOAA-11 to NOAA-14 sensor shift in the VIP3 data. Negative breaks with narrow confidence intervals are detected in semi-arid, arid and hyper-arid

regions in December 1999 (magnitudes of −0.027, −0.028 and −0.026), coinciding with the date when the VIP3 data source was changed from AVHRR to MODIS. Although the generation of VIP3 data only consists of MODIS data after 2000, clear breaks are detected in all the anomaly series except for the hyper-arid region. It is noticeable that negative breaks in February–April 2002 are detected in global, cold, dry-subhumid and semi-arid regions (magnitudes of −0.021, −0.052, −0.022 and −0.019) which are not found in the other datasets. Additionally, during the last five years breaks are detected in all averaged series except the cold region, i.e. May 2007 (magnitude = −0.027) for the global average, January 2009 (magnitude = 0.004) in the humid region, August 2009 (magnitude = 0.008) in the dry-subhumid region, December 2009 (magnitude = 0.021) in the semi-arid region, December 2009 (magnitude = 0.012) in the arid region, and August 2008 (magnitude = −0.006) in the hyper-arid region. Increasing trends are found after the last breaks in all VIP3 averaged NDVI anomaly series.

Fig. 4C shows the results of the LTDR4 data series excluding data from November 1988 to October 1989 and the years 1994 and 2000. In semi-arid and arid regions, both NOAA-7 to NOAA-9 and NOAA-9 to NOAA-11 sensor shifts coincide with detected breaks with magnitudes between −0.034 and −0.015. In the hyper-arid region, the first sensor shift also aligns with the detected break in December 1984 (magnitude = −0.007), while the second sensor shift is close to the break in May 1988 (magnitude = −0.010) but not included in the temporal coverage of the confidence interval. Breaks in the
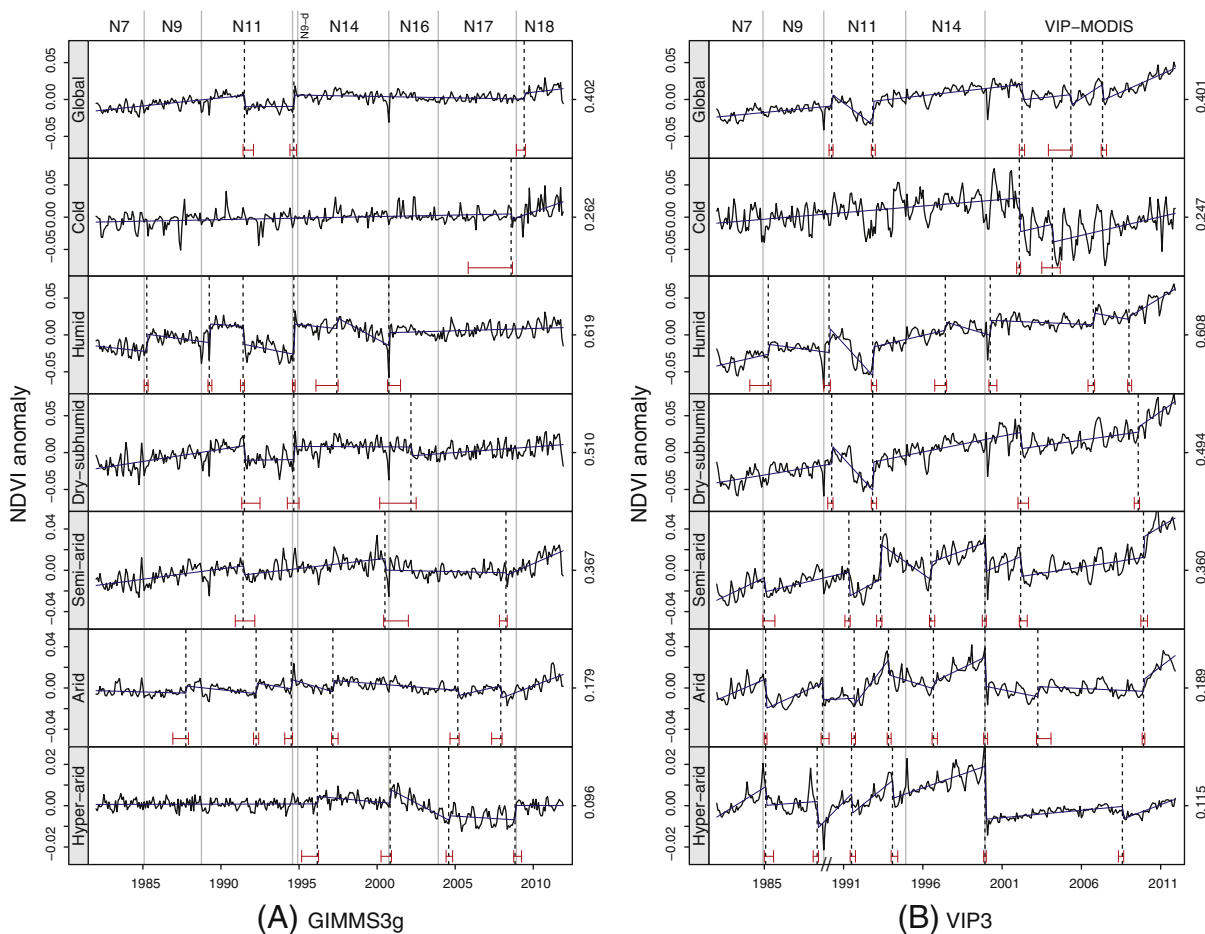
Fig. 4. Detected changes in global averaged and humidity zone averaged NDVI anomaly data from (A) GIMMS3g, (B) VIP3, (C) LTDR4, (D) SPOT-VGT, (E) MOD13C2, (F) MYD13C2, (G) LTDR-Terra, and (H) LTDR-Aqua. Mean values of each original NDVI series are indicated at the 2nd ordinate. Gray vertical lines denote platform/sensor changing time (N means NOAA). The N9-d in (A) means the NOAA-9 descending node data that GIMMS3g used during September–December 1994. Black dashed vertical lines represent the time of detected trend breaks with red error bars showing the confidence intervals of breaks. (For interpretation of the references to color in this figure legend, the reader is referred to the web version of this article.)
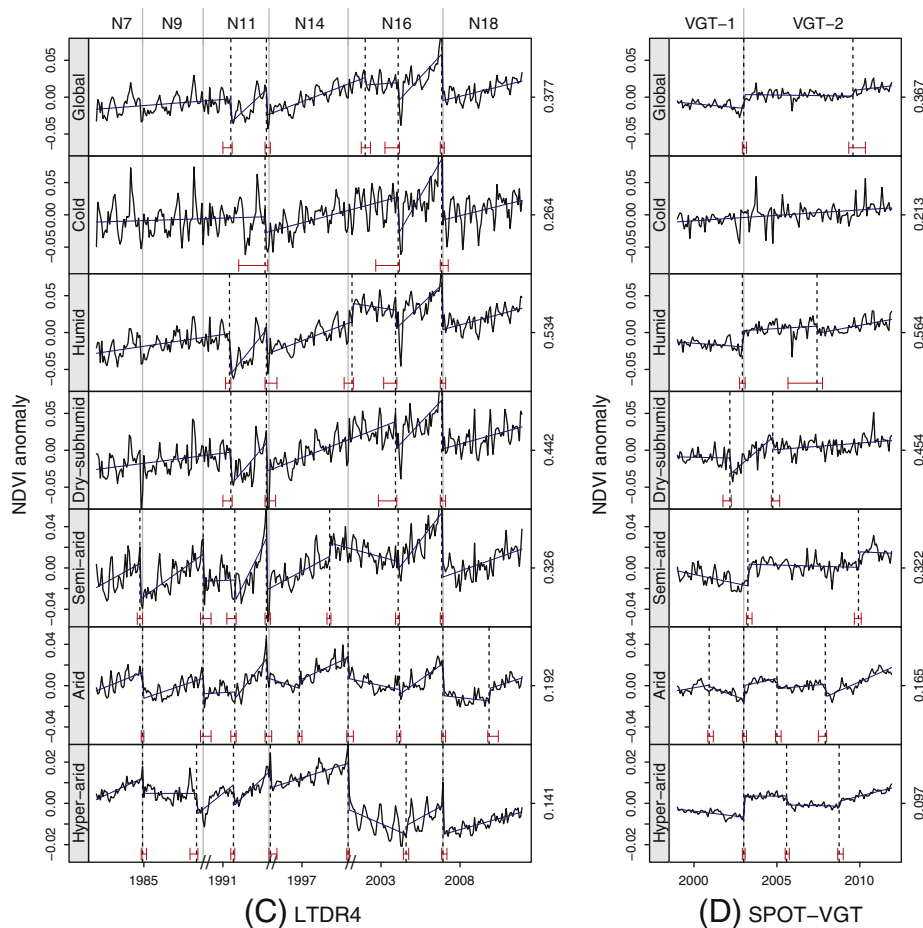
Fig. 4 (continued).

middle of 1991, coinciding with the Mt Pinatubo volcano eruption, are detected in all LTDR4 averaged series (except the cold region) with magnitudes from −0.055 to −0.005. Overlaps between sensor shift from NOAA-11 to NOAA-14 and corresponding detected breaks are found in all LTDR4 averaged series with magnitudes from −0.049 to −0.008. The NOAA-14 to NOAA-16 sensor shift coincides with breaks in humid, arid and hyper-arid regions (magnitudes of 0.025, −0.020 and −0.023). In the end of 2003/beginning of 2004, negative breaks are found in all the averaged series (except for the hyper-arid region) with magnitudes from −0.054 to −0.004 that do not coincide with a sensor shift. Whereas in the end of 2006, distinct negative breaks (magnitudes between −0.094 and −0.014) are detected in all the averaged series, coinciding with the sensor shift from NOAA-16 to NOAA-18. A break in November 2009 (magnitude = 0.012) is detected only in the arid region. Increasing trends are found in all the anomaly series from the last breaks until to the end of the time series.

Fig. 4D shows the results of the SPOT-VGT data series. Clear positive breaks are found in the beginning of 2003 in global, humid, arid and hyper-arid regions with magnitudes of 0.019, 0.022, 0.014 and 0.010, respectively, coinciding with sensor shift from VGT-1 to VGT-2. No break is detected in the cold averaged series. In the dry-subhumid region, two breaks are detected in February 2002 (magnitude = −0.021) and October 2004 (magnitude = −0.017). A positive break is found in April 2003 (magnitude = 0.021) in the semi-arid region, which is close to the sensor shift date (January 2003) but without a direct overlap with the break confidence interval. During the VGT-2 period, breaks are detected that do not coincide with sensor shift, i.e. August 2009 (magnitude = 0.008) in the global averaged series, June 2007

(magnitude = −0.009) in the humid region, December 2009 (magnitude = 0.015) in the semi-arid region, January 2005 (magnitude = −0.010) and December 2007 (magnitude = −0.012) in the arid region, and August 2005 (magnitude = −0.004) and October 2008 (magnitude = 0.003) in the hyper-arid region. No break is detected in the cold region. Increasing trends are found during the last five years in all averaged anomaly series.

Fig. 4E and F show the results of MOD13C2 and MYD14C2 data series, respectively. The MOD13C2 data shows no breakpoints or clear trends in the averaged series of global, cold, humid and dry-subhumid regions. A break is detected in September 2007 (magnitude = −0.010) in the semi-arid region, with an increasing trend afterwards. The arid region also shows a break in September 2007 (magnitude = −0.011), together with breaks in May 2003 (magnitude = 0.010), August 2005 (magnitude = −0.002) and December 2009 (magnitude = 0.008). The hyper-arid region shows breaks in January 2005 (magnitude = −0.002), October 2007 (magnitude = −0.002) and December 2009 (magnitude = 0.002). Increasing trends are found after the last breaks in arid and hyper-arid regions. Similar to the MOD13C2 data, MYD13C2 also shows no breaks or clear trends in global, cold and humid regions. Breaks in January 2005 and December 2004 with large confidence intervals and magnitudes of −0.008 are detected in dry-subhumid and semi-arid regions, respectively. A break in December 2007 (magnitude = −0.010) is found in the arid region with increasing trend afterwards. The averaged series in the hyper-arid region shows two breaks in February 2005 and October 2007, but the time series looks relatively stable due to the small magnitudes (both are −0.001) of the beaks.
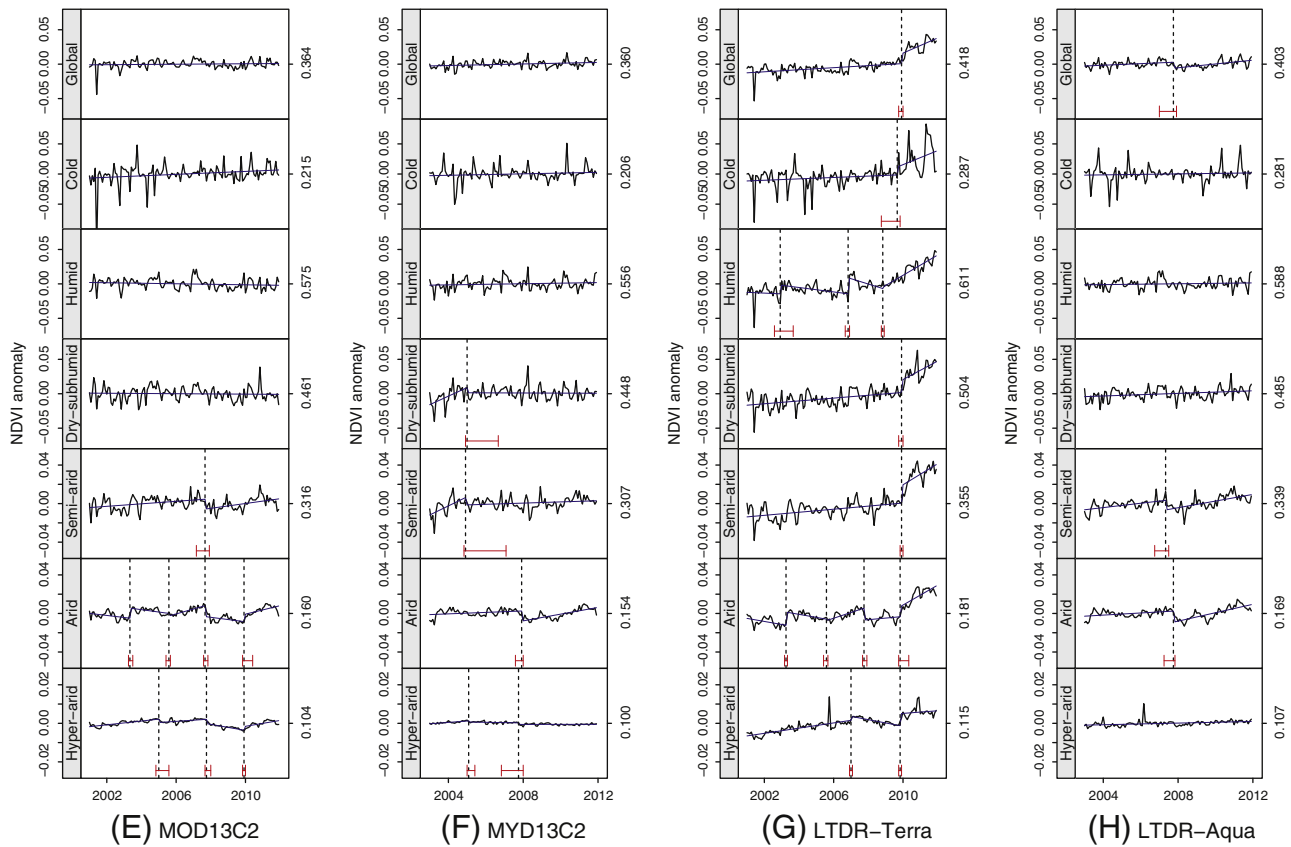
Fig. 4 (*continued*).

Fig. 4G and H shows the results of LTDR-Terra and LTDR-Aqua, respectively. LTDR-Terra data shows similar change patterns in global, cold, dry-subhumid and semi-arid regions, with only one break in 2009 (magnitudes of 0.015, 0.014, 0.019 and 0.019). Breaks in December 2002, November 2006 and November 2008 are detected in the humid region (magnitudes of 0.012, 0.023 and 0.003). The arid region has similar break positions as the MOD13C2 arid region. Two breaks in January 2007 and November 2009 are found in the hyper-arid region (magnitudes of −0.002 and 0.006). All the series data show increasing trends after the last break detected. LTDR-Aqua data shows breaks in 2007 in global, semi-arid and arid regions (magnitudes of −0.008, −0.010 and −0.011) and increasing trends afterwards. No breaks or clear trends are found in cold, humid, dry-subhumid and hyper-arid regions.

5. Discussion

5.1. Interpretation of detected breaks

It is clear from the global and regional averaged time series in Fig. 2 that the VIP3 and LTDR4 datasets are characterized by temporal inconsistencies at the beginning of the NOAA-11 time series that may be caused by unsuccessful correction of orbital drift effects. These two NDVI datasets are also suffering from severe orbital drift effects during the NOAA-7, NOAA-9, and NOAA-14 periods (Fig. 4B,C) most clearly shown in the more arid parts of the world causing higher NDVI values as a function of the equator passing time being later in the afternoon with lower solar zenith angles (Fensholt, Sandholt, Proud, Stisen, & Rasmussen, 2010). GIMMS3g also shows orbital drift effects throughout NOAA-7 to NOAA-14 in the humid region (Fig. 4A), while drift effects are not observed for the dry environments. However, it is still possible that residual orbital drift effects have caused the clear increasing trends

from 1982 to July 1991 in the dry-subhumid region. The transition from AVHRR-2 to AVHRR-3 was neither totally seamless in the GIMMS3g data or in the LTDR4 data. In addition, the LTDR4 data is also likely influenced by artifacts related to sensor shifts from NOAA-11 to NOAA-14 and from NOAA-16 to NOAA-18; the latter is evident as no breaks around this date are found in other datasets. The VIP3 data fails to produce a temporally consistent data series by using the land cover based empirical equations to convert AVHRR NDVI to the AVHRR–MODIS equivalent for the drier parts of the globe. The discontinuity of SPOT-VGT NDVI data in February 2003 was shown in Fensholt et al. (2009) and Horion et al. (2014) by examining the time series of desert transects in the Sahara. Our results further revealed that this discontinuity is also present in vegetated areas (Fig. 4D), which may be caused by radiometric differences between VGT-1 and VGT-2 being uncorrected for (VITO, 2014) and a re-processing of the entire VGT archive is foreseen in 2015. At the end of 2007/beginning of 2008 negative breaks, not related to sensor shift issues, followed by notable increasing trends were detected in arid regions of the MODIS based datasets (Fig. 4E–H) as well as GIMMS3g and SPOT-VGT datasets. The break and trend may be related to the cooling effects caused by the La Niña occurring in 2007–2008 and the following El Niño in 2009–2010, which were the strongest recorded since 2000 (Golden Gate Weather Service). Climatically driven phenology variation (from changes in temperature and moisture) is also expected to have an impact on the anomaly values (van Leeuwen, Hartfield, Miranda, & Meza, 2013). Hence, identification of modes of variation as well as significant changes within phenology could form a better basis for understanding the changes in NDVI anomalies.

5.2. Inter-comparisons between datasets and humidity zones

Both the VIP3 and LTDR4 data are produced from LTDR3 data and have quite similar NDVI anomaly change patterns around the Mt

Table 2
The magnitudes (unit: NDVI) and dates of detected breaks and the corresponding confidence intervals (2.5%–97.5%).

	GIMMS3g	VIP3	LTDR4	SPOT-VGT	MOD13C2	MYD13C2	LTDR3-Terra	LTDR3-Aqua
Global	−0.015 07/1991 (06/1991–02/1992) 0.015 09/1994 (06/1994–11/1994) 0.008 06/2009 (12/2008–07/2009)	0.015 04/1990 (02/1990–05/1990) 0.032 11/1992 (10/1992–01/1993) −0.021 04/2002 (02/2002–06/2002) −0.013 05/2005 (12/2003–06/2005) −0.021 05/2007 (04/2007–08/2007)	−0.031 07/1991 (02/1988–10/1988) −0.034 10/1993 (09/1993–01/1995) −0.010 01/2002 (10/2001–05/2002) −0.023 02/2004 (04/2003–03/2004) −0.063 11/2006 (10/2006–01/2007)	0.019 01/2003 (12/2002–03/2003) 0.008 08/2009 (05/2009–05/2010)			0.015 12/2009 (10/2009–01/2010)	−0.008 10/2007 (01/2007–12/2007)
Cold	−0.008 08/2008 (11/2005–09/2009)	−0.052 02/2002 (12/2001–03/2002) −0.027 03/2004 (07/2003–09/2004)	−0.024 09/1993 (01/1992–11/1993) −0.054 02/2004 (09/2002–03/2004) −0.094 11/2006 (10/2006–04/2007)				0.014 09/2009 (10/2008–11/2009)	
Humid	0.023 04/1985 (02/1985–05/1985) 0.025 04/1989 (03/1989–06/1989) −0.025 06/1991 (04/1991–07/1991) 0.041 09/1994 (08/1994–10/1994) 0.014 06/1997 (02/1996–07/1997) 0.017 10/2000 (09/2000–07/2001)	0.013 04/1985 (02/1984–06/1985) 0.032 02/1990 (10/1988–03/1990) 0.039 11/1992 (10/1992–02/1993) 0.011 06/1997 (10/1996–07/1997) 0.020 04/2000 (03/2000–09/2000) 0.016 10/2006 (06/2006–11/2006) 0.004 01/2009 (12/2008–03/2009)	−0.055 06/1991 (03/1991–07/1991) −0.033 10/1993 (09/1993–06/1995) 0.025 03/2001 (09/1999–04/2001) −0.024 12/2003 (03/2003–01/2004) −0.060 11/2006 (10/2006–02/2007)	0.022 12/2002 (10/2002–02/2003) −0.009 06/2007 (09/2005–10/2007)			0.012 12/2002 (08/2002–09/2003) 0.023 11/2006 (09/2006–12/2006) 0.003 11/2008 (10/2008–12/2008)	
Dry-subhumid	−0.020 07/1991 (05/1991–07/1992) 0.018 09/1994 (04/1994–01/1995) −0.012 03/2002 (03/2000–07/2002)	0.023 04/1990 (01/1990–05/1990) 0.038 11/1992 (10/1992–02/1993) −0.022 03/2002 (01/2002–09/2002)	−0.043 07/1991 (01/1991–08/1991) −0.037 10/1993 (09/1993–05/1995) −0.035 12/2003 (11/2002–01/2004)	−0.021 02/2002 (10/2001–04/2002) −0.017 10/2004 (09/2004–03/2005)		−0.008 01/2005 (12/2004–09/2006)	0.019 12/2009 (10/2009–01/2010)	

		0.008 08/2009 (05/2009–09/2009)	−0.066 11/2006 (10/2006–02/2007)					
Semi-arid	−0.009 06/1991 (12/1990–03/1992) −0.011 07/2000 (06/2000–01/2002) −0.002 04/2008 (11/2007–05/2008)	−0.013 01/1985 (12/1984–09/1985) −0.023 05/1991 (02/1991–06/1991) 0.033 05/1993 (02/1993–06/1993) 0.017 07/1996 (06/1996–10/1996) −0.027 12/1999 (10/1999–01/2000) −0.019 03/2002 (02/2002–08/2002) 0.021 12/2009 (10/2009–03/2010)	−0.034 10/1984 (08/1984–12/1984) −0.026 10/1988 (08/1988–04/1990) −0.019 10/1991 (04/1991–11/1991) −0.049 10/1993 (09/1993–01/1995) 0.013 10/1998 (08/1998–11/1998) −0.006 02/2004 (12/2003–03/2004) −0.062 11/2006 (10/2006–12/2006)	0.021 04/2003 (03/2003–07/2003) 0.015 12/2009 (09/2009–02/2010)	−0.010 09/2007 (03/2007–12/2007)	−0.008 12/2004 (11/2004–02/2007)	0.019 12/2009 (11/2009–01/2010)	−0.010 05/2007 (10/2006–07/2007)
Arid	0.007 10/1987 (12/1986–12/1987) 0.010 04/1992 (02/1992–06/1992) 0.009 07/1994 (02/1994–08/1994) 0.011 03/1997 (02/1997–07/1997) 0.005 03/2005 (09/2004–04/2005) −0.012 12/2007 (05/2007–01/2008)	−0.028 02/1985 (01/1985–03/1985) −0.016 09/1988 (08/1988–02/1990) −0.005 09/1991 (07/1991–10/1991) −0.015 11/1993 (10/1993–01/1994) 0.007 09/1996 (08/1996–12/1996) −0.028 12/1999 (11/1999–02/2000) 0.010 04/2003 (03/2003–02/2004) 0.012 12/2009 (11/2009–01/2010)	−0.025 12/1984 (11/1984–01/1985) −0.015 10/1988 (08/1988–04/1990) −0.005 10/1991 (07/1991–11/1991) −0.018 10/1993 (09/1993–02/1995) 0.008 11/1996 (10/1996–01/1997) −0.020 12/1999 (11/1999–04/2001) −0.004 03/2004 (01/2004–04/2004) −0.031 12/2006 (11/2006–02/2007) 0.012 11/2009 (10/2009–06/2010)	−0.002 12/2000 (11/2000–03/2001) 0.014 01/2003 (12/2002–03/2003) −0.010 01/2005 (12/2004–04/2005) −0.012 12/2007 (07/2007–01/2008)	0.010 05/2003 (04/2003–07/2003) −0.002 08/2005 (06/2005–09/2005) −0.011 09/2007 (08/2007–11/2007) 0.008 12/2009 (11/2009–06/2010)	−0.010 12/2007 (08/2007–01/2008)	0.013 04/2003 (03/2003–05/2003) −0.001 08/2005 (06/2005–09/2005) −0.012 10/2007 (09/2007–12/2007) 0.011 11/2009 (10/2009–05/2010)	−0.011 10/2007 (04/2007–11/2007)
Hyper-arid	0.004 03/1996 (03/1995–04/1996) 0.006 11/2000	−0.009 02/1985 (01/1985–08/1985) −0.013 05/1988	−0.007 12/1984 (11/1984–03/1985) −0.010 05/1988	0.010 01/2003 (12/2002–02/2003) −0.004 08/2005	−0.002 01/2005 (11/2004–08/2005) −0.002 10/2007	−0.001 02/2005 (01/2005–06/2005) −0.001 10/2007	0.002 01/2007 (12/2006–02/2007) 0.006 11/2009	

Table 2 (continued)

	GIMMS3g	VIP3	LTDR4	SPOT-VGT	MOD13C2	MYD13C2	LTDR3-Terra	LTDR3-Aqua
	(04/2000–12/2000)	(02/1988–06/1988)	(12/1987–06/1988)	(07/2005–10/2005)	(09/2007–01/2008)	(11/2006–01/2008)	(10/2009–12/2009)	
	0.002	−0.009	−0.010	0.003	0.002			
	08/2004	07/1991	09/1991	10/2008	12/2009			
	(06/2004–11/2004)	(06/1991–10/1991)	(07/1991–10/1991)	(09/2008–01/2009)	(11/2009–01/2010)			
	0.007	−0.008	−0.008					
	11/2008	02/1994	01/1995					
	(10/2008–04/2009)	(01/1994–06/1994)	(12/1993–06/1995)					
		−0.026	−0.023					
		12/1999	12/1999					
		(11/1999–01/2000)	(11/1999–01/2001)					
		−0.006	0.005					
		08/2008	08/2004					
		(05/2008–09/2008)	(06/2004–10/2004)					
			−0.014					
			12/2006					
			(11/2006–03/2007)					

Pinatubo volcanic eruption producing low values from the middle of 1991 to the end of 1992 in global, humid, dry-subhumid and semi-arid regions. The GIMMS3g data also showed distinct lower values from the middle of 1991 in the same regions, but the low NDVI anomalies last for a longer period until September 1994 in global, humid, and dry-subhumid regions. The GIMMS3g only corrected for the Mt Pinatubo volcanic effects until December 1993, thus the abrupt increase of NDVI anomaly in September 1994 in global, humid and dry-subhumid regions may be attributed to sensor related artifacts. In the arid region, the NDVI anomalies of GIMMS3g and VIP3/LTDR4 datasets showed different response to the Mt Pinatubo volcanic eruption. The VIP3/LTDR4 data increased significantly right after the event, which could be caused by the orbital drift effects also shown in the NOAA-7 and NOAA-9 periods. The GIMMS3g data showed no disturbance in 1991 but an abrupt increase during the following year. At the pixel level, de Jong et al. (2012) performed BFAST trend analysis based on GIMMSg data and found abrupt NDVI increases during June 1991–December 1992 in the global arid regions, i.e. Kazakhstan and West Australia. They argued that abrupt increases might be explained by the precipitation changes that counter-balanced Mt Pinatubo effects.

Terra-MODIS was reported to suffer from sensor degradation of blue, red and near-infrared bands, resulting in a NDVI decline at a rate of 0.001–0.004 per year (Wang et al., 2012). This artificially decreasing trend was shown over North America based on NDVI during July–August from 2002 to 2010. Terra MOD13C2 show smaller slope values than the Aqua MYD13C2 data in the global and humidity zone averaged monthly NDVI anomaly series (2003–2011) in the present analyses (Table 3). Particularly, the differences are >0.001 in humid and dry-subhumid regions. In addition, we further examined the seasonal based global averaged NDVI time series from 2003 to 2011 (Fig. 5). MOD13C2 shows a smaller trend (>0.001 difference per year) than MYD13C2 for averaged NDVI time series of June–August and December–February (Fig. 5A,C) which is in accordance with the results reported in Wang et al. (2012). This trend difference between MODIS sensors becomes smaller in averaged NDVI time series of September–November and March–May (<0.0005 per year) and therefore, the Terra-MODIS sensor degradation effects are less clear in the monthly NDVI time series as compared to the Northern Hemisphere growing and winter seasons. All together, these results indicate the feasibility of using globally averaged time series to examine systematic errors in satellite NDVI datasets.

It is noticeable that higher NDVI anomalies were seen for 2010–2011 in the semi-arid and arid regions of all the examined datasets, which could be caused by the enhanced land carbon sink in these areas (Poulter et al., 2014). However, a large discrepancy still exists amongst the datasets during 2010–2011. The VIP3 and LTDR-Terra datasets showed extraordinarily high NDVI anomalies for the global and all humidity zones (Fig. 4B,G), both of which were generated from Terra MODIS reflectance. While the MOD13C2 dataset, also generated from Terra MODIS reflectance, did not show such high anomalies (Fig. 4E). The GIMMS3g, LTDR4 and SPOT-VGT had similar variations during 2007–2011 and also showed higher values for 2010–2011 (Fig. 4A,C,D), but not as extreme as the VIP3 and LTDR-Terra datasets. This pattern of higher NDVI anomalies for 2010–2011 was not clearly shown in the MYD13C2 and LTDR-Aqua datasets (Fig. 4F,H). The discrepancy amongst all the datasets during recent years is somehow surprising as all of them are generated from stable platforms and improved sensors and thus are expected to be more similar. However, if we assume that the hyper-arid region should be stable over time as this region covers desert area with almost no vegetation, we find that only the MYD13C2 and LTDR-Aqua datasets meet this assumption.

Although differences amongst the MODIS based datasets exist, the magnitudes of detected breaks in NDVI anomaly series do not exceed the ± 0.011 level in MOD13C2, MYD13C2 and LTDR-Aqua.

Table 3
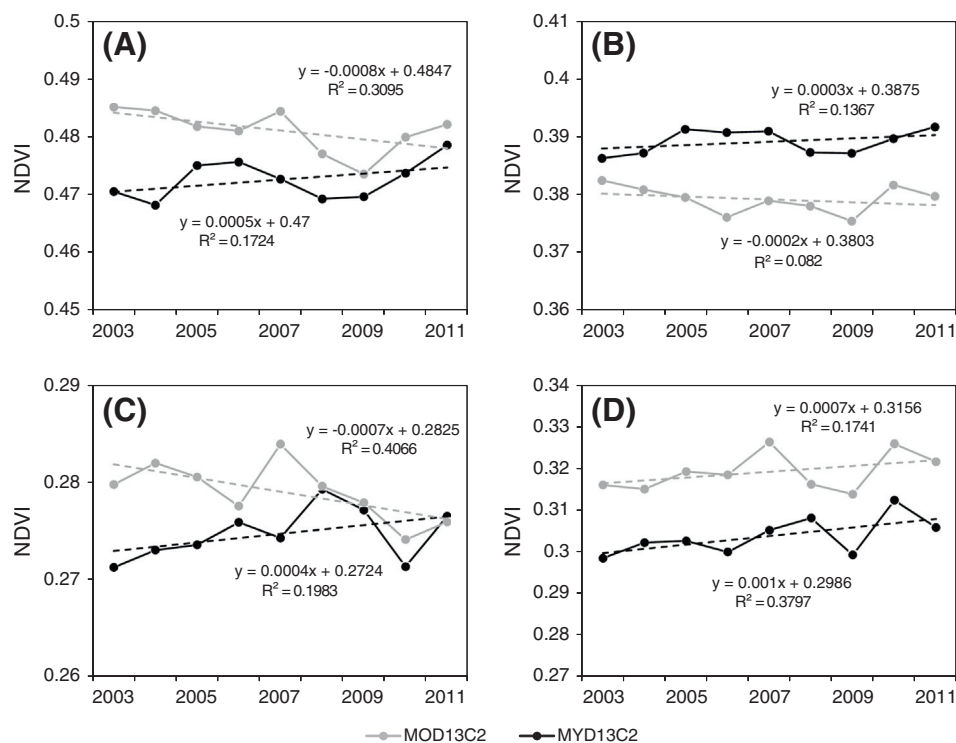Linear trends of the MOD13C2 and MYD13C2 NDVI anomaly series during 2003–2011.

Humidity zones	MOD13C2		MYD13C2		Slope difference
	Slope	R^2	Slope	R^2	
Global	− 0.00024	0.016	0.00056	0.075	− 0.00080
Cold	0.00046	0.009	0.00061	0.016	− 0.00015
Humid	− 0.00079	0.079	0.00042	0.018	− 0.00121
Dry-subhumid	− 0.00050	0.019	0.00065	0.026	− 0.00115
Semi-arid	0.00010	0.002	0.00081	0.090	− 0.00071
Arid	− 0.00008	0.002	0.00018	0.011	− 0.00026
Hyper-arid	− 0.00029	0.201	− 0.00016	0.338	− 0.00013

The GIMMS3g and SPOT-VGT datasets show roughly the same level of break magnitudes (higher than the MODIS based datasets), except for the humid region where break magnitudes in GIMMS3g exceed breaks detected in SPOT-VGT. Amongst the long-term datasets, the magnitudes of detected breaks in VIP3 and LTDR4 datasets are of higher values as compared to GIMMS3g, indicating the better temporal consistency of the GIMMS3g data.

5.3. Implications for NDVI trend analysis on pixel scale

The discontinuities caused by sensor changes in GIMMSg dataset (the previous version of GIMMS3g) were evaluated by de Jong, Verbesselt, Schaepman, and De Bruin (2011) using a per-pixel approach. Their results revealed that the temporal distribution of BFAST detected breaks reached the highest number during periods coinciding with platform changes from NOAA-9 to NOAA-11 and further from NOAA-11 to NOAA-14 (almost double amount of pixels as compared to the long term average) with high possibilities to be caused by under- or over-correction of platform changes and orbital drift. Even though a given pixel does not show breaks coinciding with platform changing dates, it cannot be concluded that this pixel was not influenced by sensor related artifacts. By averaging the data on a regional scale, our results indicate systematic artifacts in the humid region.

Therefore, it could be problematic to use the GIMMS3g NDVI data for vegetation trend analysis in humid parts of the world. No evidence of temporal inconsistencies was found for the GIMMS3g data in the arid region; hence trend analysis based on GIMMS3g data in arid regions should have high reliability. For the semi-arid region, the discontinuity of sensor shifts from NOAA-14 to NOAA-16 should be treated with caution when performing trend analysis covering this time. As The El Chichon volcanic eruption should affect the NDVI values negatively like the Mt Pinatubo volcano and the influence period (March 1982–December 1984) is at the beginning of the GIMMS3g time span, it may contribute to the greening trends in the global semi-arid region reported in Fensholt et al. (2012) and Helldén and Tottrup (2008). Whether this period of low NDVI values coinciding with the El Chichon volcanic eruption, should be considered as an artifact or the eruption actually caused a real decrease in NDVI due to changed climatic forcing (Lucht et al., 2002) cannot be concluded from this study. The sensor shift related breaks in SPOT-VGT data series would introduce an increasing trend in NDVI. This was confirmed by Guay et al. (2014) who conducted per-pixel trend analysis and compared growing season NDVI from GIMMSg, GIMMS3g, MODIS, and SPOT-VGT data during 2002–2008 at high northern latitudes (>50°N) and found widespread greening trends only in the SPOT-VGT based results. Trend analysis results from GIMMS3g, SPOT-VGT and Terra-MODIS based datasets covering the years of 2010–2011 should be interpreted with caution because of the unrealistic higher NDVI anomalies in the hyper-arid region averaged series. The VIP3 and LTDR4 datasets should not be used for long-term NDVI trend analysis in the global drylands due to severe temporal inconsistencies between sensors. However, this does not mean that these two datasets cannot be used for other applications e.g. related to long-term monitoring of vegetation phenology. Parameterization of the onset, peak time and end of season can still be well captured and is expected to be less impacted from abrupt shifts in time series as compared to impacts from shifts on linear trend analysis (Scheftic, Zeng, Broxton, & Brunke, 2014; van Leeuwen & Hartfield, 2013).

Fig. 5. Linear trends of global averaged MOD13C2 and MYD13C2 NDVI time series (2003–2011), averaged (A) from June to August, (B) from September to November, (C) from December to February, and (D) from March to May.

6. Conclusions

We evaluated the temporal consistency of GIMMS3g, LTDR4, VIP3, and SPOT-VGT datasets. The global land surface area is divided into six regions according to the world humidity zones and averaged NDVI time series are calculated and analyzed in each region for all the candidate datasets. GIMMS3g NDVI data showed an inconsistency between sensors in humid, dry-subhumid, semi-arid and hyper-arid regions. VIP3 and LTDR4 datasets showed clear artifacts at the beginning of NOAA-11 and orbital drift effects in semi-arid, arid and hyper-arid regions during 1982–2000. In addition, VIP3 and LTDR4 showed data inconsistencies when changing the data source from AHVRR to MODIS and from NOAA-16 to NOAA-18, respectively. Amongst the long-term AVHRR based datasets analyzed, the GIMMS3g is found to have the highest temporal consistency and at present state will be the most appropriate choice for NDVI trend analysis. The discontinuity between VGT-1 and VGT-2 at the beginning of 2003 in SPOT-VGT NDVI dataset is clearly seen and impacts trend analysis for all vegetated regions. Distinct different NDVI values amongst the examined datasets during 2010–2011 have resulted in different vegetation breaks and trends for recent years. The reasons behind these discrepancies need to be further explored since a growing volume of studies within vegetation and climate change research is based on these long term datasets.

References

Alcaraz-Segura, D., Chuvieco, E., Epstein, H.E., Kasischke, E.S., & Trishchenko, A. (2010a). Debating the greening vs. browning of the North American boreal forest: differences between satellite datasets. *Global Change Biology, 16*, 760–770.

Alcaraz-Segura, D., Liras, E., Tabik, S., Paruelo, J., & Cabello, J. (2010b). Evaluating the consistency of the 1982–1999 NDVI trends in the Iberian Peninsula across four time-series derived from the AVHRR Sensor: LTDR, GIMMS, FASIR, and PAL-II. *Sensors, 10*, 1291–1314.

Anyamba, A., & Eastman, J.R. (1996). Interannual variability of NDVI over Africa and its relation to El Nino Southern Oscillation. *International Journal of Remote Sensing, 17*, 2533–2548.

Bai, J. (1997). Estimation of a change point in multiple regression models. *Review of Economics and Statistics, 79*, 551–563.

Bai, Z.G., Dent, D.L., Olsson, L., & Schaepman, M.E. (2008). Proxy global assessment of land degradation. *Soil Use and Management, 24*, 223–234.

Bai, J., & Perron, P. (2003). Computation and analysis of multiple structural change models. *Journal of Applied Econometrics, 18*, 1–22.

Barreto-Munoz, A. (2013). *Multi-sensor vegetation index and land surface phenology earth science data records in support of global change studies: Data quality challenges and data explorer system.* (Ph.D. Thesis) Tucson, AZ, USA: The University of Arizona (http://arizona.openrepository.com/arizona/bitstream/10150/301661/1/azu_etd_12902_sip1_m.pdf).

Beck, H.E., McVicar, T.R., van Dijk, A.I.J.M., Schellekens, J., de Jeu, R.A.M., & Bruijnzeel, L.A. (2011). Global evaluation of four AVHRR–NDVI data sets: Intercomparison and assessment against Landsat imagery. *Remote Sensing of Environment, 115*, 2547–2563.

Boschetti, M., Nutini, F., Brivio, P.A., Bartholomé, E., Stroppiana, D., & Hoscilo, A. (2013). Identification of environmental anomaly hot spots in West Africa from time series of NDVI and rainfall. *ISPRS Journal of Photogrammetry and Remote Sensing, 78*, 26–40.

Brown, M.E., Pinzon, J.E., Didan, K., Morisette, J.T., & Tucker, C.J. (2006). Evaluation of the consistency of long-term NDVI time series derived from AVHRR, SPOT-vegetation, SeaWiFS, MODIS, and Landsat ETM+ sensors. *IEEE Transactions on Geoscience and Remote Sensing, 44*, 1787–1793.

de Beurs, K.M., & Henebry, G.M. (2004). Trend analysis of the Pathfinder AVHRR land (PAL) NDVI data for the deserts of central Asia. *IEEE Geoscience and Remote Sensing Letters, 1*, 282–286.

de Beurs, K.M., & Henebry, G.M. (2005). A statistical framework for the analysis of long image time series. *International Journal of Remote Sensing, 26*, 1551–1573.

de Jong, R., Verbesselt, J., Schaepman, M.E., & De Bruin, S. (2011). Detection of breakpoints in global NDVI time series. *34th International Symposium on Remote Sensing of Environment (ISRSE). Sydney, Australia.*

de Jong, R., Verbesselt, J., Schaepman, M.E., & de Bruin, S. (2012). Trend changes in global greening and browning: Contribution of short-term trends to longer-term change. *Global Change Biology, 18*, 642–655.

Didan, K. (2010). Multi-satellite earth science data record for studying global vegetation trends and changes. *Proceedings of the 2010 International Geoscience and Remote Sensing Symposium. Honolulu, HI, USA.*

Fensholt, R., Langanke, T., Rasmussen, K., Reenberg, A., Prince, S.D., Tucker, C., et al. (2012). Greenness in semi-arid areas across the globe 1981–2007 — An Earth observing satellite based analysis of trends and drivers. *Remote Sensing of Environment, 121*, 144–158.

Fensholt, R., & Proud, S.R. (2012). Evaluation of earth observation based global long term vegetation trends — Comparing GIMMS and MODIS global NDVI time series. *Remote Sensing of Environment, 119*, 131–147.

Fensholt, R., Rasmussen, K., Nielsen, T.T., & Mbow, C. (2009). Evaluation of earth observation based long term vegetation trends — Intercomparing NDVI time series trend analysis consistency of Sahel from AVHRR GIMMS, Terra MODIS and SPOT VGT data. *Remote Sensing of Environment, 113*, 1886–1898.

Fensholt, R., Sandholt, I., Proud, S.R., Stisen, S., & Rasmussen, M.O. (2010). Assessment of MODIS sun-sensor geometry variations effect on observed NDVI using MSG SEVIRI geostationary data. *International Journal of Remote Sensing, 31*, 6163–6187.

Fernandes, R., & Leblanc, S.G. (2005). Parametric (modified least squares) and non-parametric (Theil–Sen) linear regressions for predicting biophysical parameters in the presence of measurement errors. *Remote Sensing of Environment, 95*, 303–316.

Forkel, M., Carvalhais, N., Verbesselt, J., Mahecha, M.D., Neigh, C.S.R., & Reichstein, M. (2013). Trend change detection in NDVI time series: Effects of inter-annual variability and methodology. *Remote Sensing, 5*, 2113–2144.

Gideon, S. (1978). Estimating the dimension of a model. *The Annals of Statistics, 6*, 461–464.

Goetz, S.J., Fiske, G.J., & Bunn, A.G. (2006). Using satellite time-series data sets to analyze fire disturbance and forest recovery across Canada. *Remote Sensing of Environment, 101*, 352–365.

Golden Gate Weather Services (s). El Niño and La Niña years and intensities. http://ggweather.com/enso/oni.htm

Guay, K.C., Beck, P.S.A., Berner, L.T., Goetz, S.J., Baccini, A., & Buermann, W. (2014). Vegetation productivity patterns at high northern latitudes: A multi-sensor satellite data assessment. *Global Change Biology, 20*, 3147–3158.

Helldén, U., & Tottrup, C. (2008). Regional desertification: A global synthesis. *Global and Planetary Change, 64*, 169–176.

Holben, B.N. (1986). Characteristics of maximum-value composite images from temporal AVHRR data. *International Journal of Remote Sensing, 7*, 1417–1434.

Horion, S., Fensholt, R., Tagesson, T., & Ehammer, A. (2014). Using earth observation-based dry season NDVI trends for assessment of changes in tree cover in the Sahel. *International Journal of Remote Sensing, 35*, 2493–2515.

Huete, A., Didan, K., Miura, T., Rodriguez, E.P., Gao, X., & Ferreira, L.G. (2002). Overview of the radiometric and biophysical performance of the MODIS vegetation indices. *Remote Sensing of Environment, 83*, 195–213.

Ivits, E., Horion, S., Fensholt, R., & Cherlet, M. (2014). Drought footprint on European ecosystems between 1999 and 2010 assessed by remotely sensed vegetation phenology and productivity. *Global Change Biology, 20*, 581–593.

Jamali, S., Jönsson, P., Eklundh, L., Ardö, J., & Seaquist, J. (2015). Detecting changes in vegetation trends using time series segmentation. *Remote Sensing of Environment, 156*, 182–195.

Jamali, S., Seaquist, J., Eklundh, L., & Ardö, J. (2014). Automated mapping of vegetation trends with polynomials using NDVI imagery over the Sahel. *Remote Sensing of Environment, 141*, 79–89.

James, M.E., & Kalluri, S.N.V. (1994). The Pathfinder AVHRR land data set: An improved coarse resolution data set for terrestrial monitoring. *International Journal of Remote Sensing, 15*, 3347–3363.

Lambert, J., Drenou, C., Denux, J. -P., Balent, G., & Cheret, V. (2013). Monitoring forest decline through remote sensing time series analysis. *GIScience & Remote Sensing, 50*, 437–457.

Latifovic, R., Pouliot, D., & Dillabaugh, C. (2012). Identification and correction of systematic error in NOAA AVHRR long-term satellite data record. *Remote Sensing of Environment, 127*, 84–97.

Li, Z.T., & Kafatos, M. (2000). Interannual variability of vegetation in the United States and its relation to El Nino/Southern Oscillation. *Remote Sensing of Environment, 71*, 239–247.

Los, S.O. (1998). Estimation of the ratio of sensor degradation between NOAA AVHRR channels 1 and 2 from monthly NDVI composites. *IEEE Transactions on Geoscience and Remote Sensing, 36*, 206–213.

Los, S.O. (2013). Analysis of trends in fused AVHRR and MODIS NDVI data for 1982–2006: Indication for a CO_2 fertilization effect in global vegetation. *Global Biogeochemical Cycles, 27*, 318–330.

Los, S.O., Collatz, G.J., Sellers, P.J., Malmstrom, C.M., Pollack, N.H., DeFries, R.S., et al. (2000). A global 9-yr biophysical land surface dataset from NOAA AVHRR data. *Journal of Hydrometeorology, 1*, 183–199.

Lucht, W., Prentice, I.C., Myneni, R.B., Sitch, S., Friedlingstein, P., Cramer, W., et al. (2002). Climatic control of the high-latitude vegetation greening trend and Pinatubo effect. *Science, 296*, 1687–1689.

Maisongrande, P., Duchemin, B., & Dedieu, G. (2004). VEGETATION/SPOT: An operational mission for the earth monitoring; presentation of new standard products. *International Journal of Remote Sensing, 25*, 9–14.

Mao, J., Shi, X., Thornton, P.E., Hoffman, F.M., Zhu, Z., & Myneni, R.B. (2013). Global latitudinal-asymmetric vegetation growth trends and their driving mechanisms: 1982–2009. *Remote Sensing, 5*, 1484–1497.

Martínez, B., & Gilabert, M.A. (2009). Vegetation dynamics from NDVI time series analysis using the wavelet transform. *Remote Sensing of Environment, 113*, 1823–1842.

Nagaraja Rao, C.R., & Chen, J. (1995). Inter-satellite calibration linkages for the visible and near-infared channels of the advanced very high resolution radiometer on the NOAA-7, -9, and -11 spacecraft. *International Journal of Remote Sensing, 16*, 1931–1942.

Nagaraja Rao, C.R., & Chen, J. (1996). Post-launch calibration of the visible and near-infrared channels of the advanced very high resolution radiometer on the NOAA-14 spacecraft. *International Journal of Remote Sensing, 17*, 2743–2747.

Pedelty, J., Devadiga, S., Masuoka, E., Brown, M., Pinzon, J., Tucker, C., et al. (2007). Generating a long-term land data record from the AVHRR and MODIS instruments. *Geoscience and Remote Sensing Symposium, 2007. IGARSS 2007* (pp. 1021–1025). IEEE International.

Pinzon, J., Brown, M.E., & Tucker, C.J. (2005). Satellite time series correction of orbital drift artifacts using empirical mode decomposition. In N. Huang (Ed.), *Hilbert–Huang transform: Introduction and applications* (pp. 167–186).

Pinzon, J., & Tucker, C. (2014). A non-stationary 1981–2012 AVHRR NDVI3g time series. *Remote Sensing, 6*, 6929–6960.

Poulter, B., Frank, D., Ciais, P., Myneni, R.B., Andela, N., Bi, J., et al. (2014). Contribution of semi-arid ecosystems to interannual variability of the global carbon cycle. *Nature, 509*, 600–603.

Prince, S.D. (1991). A model of regional primary production for use with coarse resolution satellite data. *International Journal of Remote Sensing, 12*, 1313–1330.

Rahman, H., & Dedieu, G. (1994). SMAC: A simplified method for the atmospheric correction of satellite measurements in the solar spectrum. *International Journal of Remote Sensing, 15*, 123–143.

Rasmussen, K., Fensholt, R., Fog, B., Rasmussen, L.V., & Yanogo, I. (2014). Explaining NDVI trends in northern Burkina Faso. *Geografisk Tidsskrift-Danish Journal of Geography, 114*, 17–24.

Schaaf, C.B., Gao, F., Strahler, A.H., Lucht, W., Li, X.W., Tsang, T., et al. (2002). First operational BRDF, albedo nadir reflectance products from MODIS. *Remote Sensing of Environment, 83*, 135–148.

Scheftic, W., Zeng, X.B., Broxton, P., & Brunke, M. (2014). Intercomparison of seven NDVI Products over the United States and Mexico. *Remote Sensing, 6*, 1057–1084.

Schucknecht, A., Erasmi, S., Niemeyer, I., & Matschullat, J. (2013). Assessing vegetation variability and trends in north-eastern Brazil using AVHRR and MODIS NDVI time series. *European Journal of Remote Sensing, 46*, 40–59.

Solano, R., Didan, K., Jacobson, A., & Huete, A. (2010). MODIS vegetation index user's guide (MOD13 series). http://vip.arizona.edu/documents/MODIS/MODIS_VI_UsersGuide_01_2012.pdf

Tucker, C.J. (1979). Red and photographic infrared linear combinations for monitoring vegetation. *Remote Sensing of Environment, 8*, 127–150.

Tucker, C.J., Pinzon, J.E., Brown, M.E., Slayback, D.A., Pak, E.W., Mahoney, R., et al. (2005). An extended AVHRR 8-km NDVI dataset compatible with MODIS and SPOT vegetation NDVI data. *International Journal of Remote Sensing, 26*, 4485–4498.

Tucker, C.J., Vanpraet, C.L., Sharman, M.J., & Van Ittersum, G. (1985). Satellite remote sensing of total herbaceous biomass production in the Senegalese sahel: 1980–1984. *Remote Sensing of Environment, 17*, 233–249.

UNEP, Middleton, N.J., & Thomas, D.S.G. (1997). *World atlas of desertification* (2nd ed.). London: America by John Wiley. New York, copublished in the US, Central and South.

van Leeuwen, W., & Hartfield, K. (2013). *Trends and ENSO/AAO driven variability in productivity and phenology in South America: Comparing NDVI-VIP and NDVI3g results.* VIP Workshop. Tucson, USA: University of Arizona (http://measures.arizona.edu/documents/workshop/docs/measures_project/WORKSHOP_WvL_KH.pdf).

van Leeuwen, W.J.D., Hartfield, K., Miranda, M., & Meza, F.J. (2013). Trends and ENSO/AAO driven variability in NDVI derived productivity and phenology alongside the Andes Mountains. *Remote Sensing, 5*, 1177–1203.

van Leeuwen, W.J.D., Orr, B.J., Marsh, S.E., & Herrmann, S.M. (2006). Multi-sensor NDVI data continuity: Uncertainties and implications for vegetation monitoring applications. *Remote Sensing of Environment, 100*, 67–81.

Verbesselt, J., Hyndman, R., Newnham, G., & Culvenor, D. (2010a). Detecting trend and seasonal changes in satellite image time series. *Remote Sensing of Environment, 114*, 106–115.

Verbesselt, J., Hyndman, R., Zeileis, A., & Culvenor, D. (2010b). Phenological change detection while accounting for abrupt and gradual trends in satellite image time series. *Remote Sensing of Environment, 114*, 2970–2980.

Vermote, E.F., El Saleous, N.Z., & Justice, C.O. (2002). Atmospheric correction of MODIS data in the visible to middle infrared: first results. *Remote Sensing of Environment, 83*, 97–111.

Vermote, E., & Kaufman, Y.J. (1995). Absolute calibration of AVHRR visible and near-infrared channels using ocean and cloud views. *International Journal of Remote Sensing, 16*, 2317–2340.

Vermote, E., Saleous, N.E., Kaufman, Y.J., & Dutton, E. (1997). Data pre-processing: Stratospheric aerosol perturbing effect on the remote sensing of vegetation: Correction method for the composite NDVI after the Pinatubo eruption. *Remote Sensing Reviews, 15*, 7–21.

VITO (2014). SPOT vegetation FAQ (frequently asked questions). http://www.vgt.vito.be/faqnew/index.html

Wang, D., Morton, D., Masek, J., Wu, A., Nagol, J., Xiong, X., et al. (2012). Impact of sensor degradation on the MODIS NDVI time series. *Remote Sensing of Environment, 119*, 55–61.

Watts, L.M., & Laffan, S.W. (2014). Effectiveness of the BFAST algorithm for detecting vegetation response patterns in a semi-arid region. *Remote Sensing of Environment, 154*, 234–245.

Wessels, K.J., van den Bergh, F., & Scholes, R.J. (2012). Limits to detectability of land degradation by trend analysis of vegetation index data. *Remote Sensing of Environment, 125*, 10–22.

Xiong, X.X., & Barnes, W. (2006). An overview of MODIS radiometric calibration and characterization. *Advances in Atmospheric Sciences, 23*, 69–79.

Yin, H., Udelhoven, T., Fensholt, R., Pflugmacher, D., & Hostert, P. (2012). How normalized difference vegetation index (NDVI) trends from advanced very high resolution radiometer (AVHRR) and Système Probatoire d'Observation de la Terre VEGETATION (SPOT VGT) time series differ in agricultural areas: An inner Mongolian case study. *Remote Sensing, 4*, 3364–3389.

Zeileis, A., & Kleiber, C. (2005). Validating multiple structural change models — A case study. *Journal of Applied Econometrics, 20*, 685–690.

Zeileis, A., Kleiber, C., Krämer, W., & Hornik, K. (2003). Testing and dating of structural changes in practice. *Computational Statistics & Data Analysis, 44*, 109–123.

Zeileis, A., Leisch, F., Hornik, K., & Kleiber, C. (2002). strucchange: An R package for testing for structural change in linear regression models. *Journal of Statistical Software, 7*, 1–38.